Active Antenna Design for Lunar-Based Detection of Global 21cm-Signals from the Dark Ages

Active Antenna Design for Lunar-Based Detection of Global 21cm-signals from the Dark Ages

J.C.F. Zandboer*, D.S. Prinsloo*†, U. Johannsen*†, M.J. Bentum*†
*Department of Electrical Engineering, Eindhoven University of Technology, Eindhoven, The Netherlands
†Netherlands Institute for Radio Astronomy, Dwingeloo, The Netherlands
j.c.f.zandboer@tue.nl

***Abstract*— This paper concerns the parameters, simulations and techniques involved in designing an active antenna system for detection of global 21cm-signals originating from the Dark Ages at the Lunar far side. A 10.5 m diameter equiangular spiral plate antenna is fashioned to operate from 10 to 70 MHz whilst maintaining a virtually frequency-independent impedance characteristic and radiation pattern. Combined with the stable and low noise performance of the measured PHA-13LN+ amplifier evaluation board, the simulations show that the full active antenna system is well suited to the science objective of this paper.**

***Index Terms*—broadband antennas, low-noise amplifiers, noise measurement, radio astronomy, space technology, Moon**

I. Introduction

ONE of humanity's most intriguing questions has always been: *"Where do we come from?"*. Through the study of signals and traces from the past, parts of the history of our universe have been unraveled. There is, however, a specific period of which still very little is known: the Dark Ages. It marks the period after the Big Bang and before the first stars when the universe was filled with neutral hydrogen.

A promising way to probe the Dark Ages is the 21cm-line predicted by the standard Lambda-Cold Dark Matter (ΛCDM) Model of Cosmology [1]. Over time, the absorption or emission by hydrogen of electromagnetic (EM) radiation with a wavelength of 21 cm [2] against the Cosmic Microwave Background (CMB) reference creates a redshifted spectrum that can serve as a global indicator of the conditions during the Dark Ages, the timing of the Cosmic Dawn and the evolution of the universe until the hydrogen interaction disappears [1].

However, foreground radiation, redshift below 100 MHz, and ionospheric attenuation make it difficult to measure the 21cm-signals today. As a result, carefully characterized equipment, long measurement campaigns, and extensive foreground mitigation techniques are required. A useful feature for this is that the 21cm-line is expected to be uniform over large scales (i.e. global) and unpolarized compared to the spatially varying (i.e. local) and polarized foreground emission [3].

Several attempts have been made to measure the Dark Ages signal on Earth, most notably the Experiment to Detect the Global EoR Signature (EDGES) [4]. Despite a careful calibration strategy [5], the deviation of EDGES from the expected ΛCDM model and other observations [6] shows the need for an independent verification away from possible terrestrial disturbances, [7] and references therein.

As a result, the Netherlands Institute for Radio Astronomy (ASTRON) in collaboration with the Eindhoven University of Technology (TU/e), the Radboud Radio Lab (RRL), the European Space Agency (ESA) and other partners is pushing for a new measurement campaign in space. It is envisioned that a standalone instrument within the future Astrophysical Lunar Observatory (ALO) [8] could perform measurements of the global 21cm-line from the only place in the inner solar system shielded from human-made radio-frequency interference (RFI) generated on Earth: the far side of the Moon [9].

This paper revolves around the question of how to design such an active antenna for Lunar global 21cm-signals detection. Sec. II starts with a description of the Lunar environment. The active antenna design parameters are introduced in Sec. III. After this, the analysis is split up into Sec. IV for the antenna design and Sec. V for the amplifier noise characterization before converging in Sec. VI by presenting the full active antenna simulation results.

II. Lunar Environment

Lunar regolith is a general name for the rocky debris that covers the Moon. As shown in [10], the cratered Lunar surface is a collection of darker mare areas and lighter highland regions. Because of these geological differences, the dielectric properties of the Moon are still largely unknown. Therefore, an educated guess is made based on the 132 Lunar samples of Tab. A9.16 in [11]. As dielectric constant, the median value $\varepsilon_{\mathrm{r}} = 3.21$ is chosen. The loss-tangent is set at $\tan\delta = 0.02$. This means that approximately 85% of the Lunar samples has an equal or lower value. The simulated antenna will be placed on top of a dielectric half-space (DHS) instead of a full free space (FS) environment to model the regolith properties.

III. Active Antenna Design Parameters

An active antenna consists of an antenna combined with an amplifier. In order to perform the 21cm-line measurement, several parameters and requirements need to be considered.

A. Frequency Invariant Characteristics

One of the biggest challenges for the active antenna design is that all contributors to the measurement read-out should be accurately known. In fact, foreground mitigation techniques, next to foreground radiation information, rely on an extremely predictable (i.e. stable and reproducible) active antenna. Any

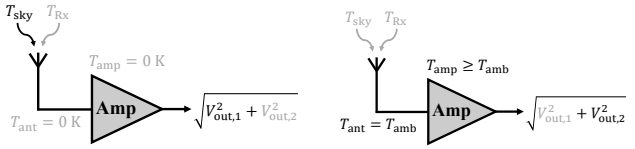

(a) Determine transfer function.

(b) Calculate receiver noise output.

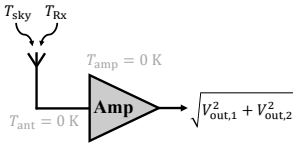

(c) Calculate temperature.

Fig. 1. The conceptual steps (a,b,c) to determine the equivalent isotropic noise temperature of the active antenna. Disabled components are grayed out.

uncertainty or large fluctuations could result in mistaking measurement artifacts for a Dark Ages feature. However, it is unavoidable that the unpredictable Lunar environment will influence the frequency response of the active antenna. To ensure a stable measurement read-out, it is therefore required to design an extremely frequency-invariant active antenna.

B. Equivalent Isotropic Noise Temperatures

Next to a frequency invariant response, the foreground mitigation techniques require the noise added by the active antenna to be lower than the received galactic radiation (i.e. it is the receiver noise, not the system noise, that should be minimized). Therefore, it is common in astronomical applications to use the equivalent isotropic receiver noise temperature T_{Rx} in comparison with the equivalent isotropic sky noise temperature T_{sky} as a figure of merit (FoM). This translates into the goal to achieve

$$T_{\text{Rx}} < T_{\text{sky}}. \tag{1}$$

Bear in mind that although it is not shown in the equations, all design parameters and variables can be frequency-dependent.

In [12] an approximation for T_{sky} is given. As noise generated by the Lunar regolith is assumed to be insignificant compared to the galactic noise, this approximation can directly be used. Determining the value of T_{Rx} is more involved as it requires the transformation of all noise contributions in the active antenna to the isotropic sky noise reference frame. The process is visualized in Fig. 1. The schematics show the various noise components involved in the active antenna with T_{amb} being the ambient temperature.

The first step is to determine the transfer function H through

$$H = \frac{V_{\text{out,1}}}{V_{\text{n,sky}}}, \tag{2}$$

where $V_{\text{out,1}}$ is the voltage noise spectral density (henceforth referred to as noise voltage) at the output of the system when only the sky noise is considered as input. The receiver itself is assumed to be noiseless. $V_{\text{n,sky}}$ is the noise voltage related to a sky noise temperature of T_{sky} via

$$V_{\text{n,sky}} = \sqrt{4k_{\text{B}}T_{\text{sky}}R_{\text{rad}}}, \tag{3}$$

TABLE I
DESIGN PARAMETERS LOG-SPIRAL ANTENNA

Parameter	Symbol	Value
Inner diameter	D_{i}	1.36 m
Outer diameter	D_{o}	9.54 m
Full diameter	D_{g}	10.5 m
Angular arm width	δ	90°
Number of turns	N	1.5
Thickness	t	35 µm
Material	-	Cu
Height above DHS	h	1 cm

where k_{B} is the Boltzmann constant and R_{rad} the antenna radiation resistance. As (3) is used to obtain a transfer function, the value of T_{sky} is irrelevant and is often set to $T_{\text{sky}} = 1$ K.

The next step, illustrated in Fig. 1b, is to determine the output noise voltage $V_{\text{out,2}}$ when only considering the receiver noise. This means setting $T_{\text{sky}} = 0$ K, introducing noisy components ($T_{\text{amb}} > 0$ K) and using the generated noise voltages to calculate the output noise voltage.

Using the results of steps 1 and 2, the equivalent isotropic noise temperature of the receiver can be calculated through

$$T_{\text{Rx}} = \frac{|V_{\text{out,2}}|^2}{4k_{\text{B}}R_{\text{rad}}|H|^2}. \tag{4}$$

Fig. 1c shows this T_{Rx} represents the sky-referred noise generated by the receiver to be used in comparison to T_{sky}.

C. Additional Antenna Parameters

In order to use foreground mitigation techniques, the antenna should have extremely frequency-invariant characteristics. A high gain is not required. On the contrary, an antenna with a lower gain and wider field-of-view (FOV) allows one to simultaneously measure a larger portion of the sky and reduce the impact of strong but local foreground radiation.

Sec. I mentions that the 21cm-line has been redshifted below 100 MHz. Based on Fig. 1 of [13], this notion is put into the requirement that the antenna should maintain the discussed characteristics from 10 to 70 MHz (i.e. a 1:7 bandwidth). This is a minimum, it is preferable to have out-of-band stability for other frequencies below 100 MHz as well.

Lastly, the fact that the active antenna should be placed on the Moon poses restrictions on its size, geometry and weight.

IV. ANTENNA DESIGN

In this work, the possibility of using an equiangular spiral plate antenna (henceforth called log-spiral antenna) is investigated. Not only does it, in theory, have extremely frequency invariant characteristics, it is also a 2D structure making it easier to deploy on the Lunar surface.

Fig. 2 shows the log-spiral antenna design created in the Altair Feko software suite [14] with its parameters listed in Tab. I. The values are based on [15] and [16], with 10 MHz and 70 MHz as minimum and maximum operating frequency, respectively. An even broader bandwidth can be obtained by increasing the outer diameter or decreasing the inner diameter of the spiral. The circular design also means the radiation pattern of the antenna only rotates with frequency, making

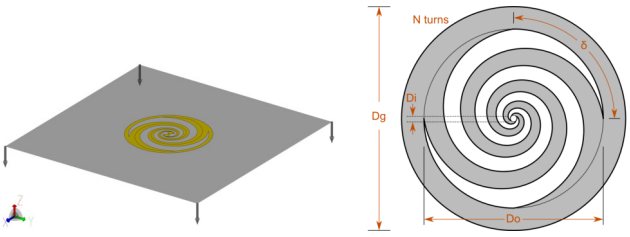

(a) (b)

Fig. 2. The copper log-spiral antenna of Tab. I above a dielectric half-space simulating the Lunar regolith (a). The schematic showing the general parameters (b) is retrieved from [17].

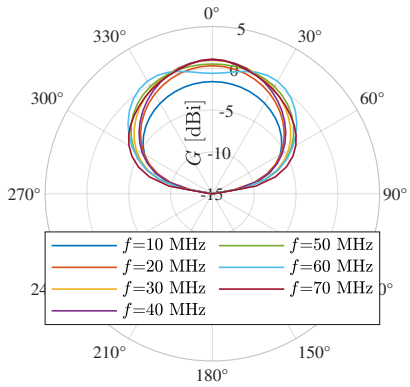

Fig. 3. The total far field gain of the log-spiral antenna as shown in Fig. 2 for $\varphi = 0°$ and varying θ at various frequencies.

it virtually frequency invariant. Unless stated otherwise, the DHS shown in Fig. 2a has the dielectric properties of Sec. II.

Fig. 3 shows the simulated total far field gain for various frequencies. It clearly illustrates that all EM radiation into the simulated regolith is fully absorbed by the lossy DHS. Next to that, the radiation pattern remains stable over the full frequency range with a slight deformation starting to appear at the higher end. The maximum variation over frequency is 2.7 dB in gain and 26° in half power beamwidth (HPBW).

The real and imaginary simulated antenna impedance, R_{ant} and X_{ant}, as well as the two components of the real impedance: the loss resistance, R_{loss}, and the radiation resistance, R_{rad}, are shown in Fig. 4. From the figure, it can be concluded that, in accordance with theory, the in-band impedance is extremely stable over frequency. However, the absolute value of the impedance is lower compared to FS and most of R_{ant} is consumed by R_{loss} due to the copper and regolith. Although the low antenna efficiency negatively affects the noise characteristics of the antenna, its stable response is more important for the overall active antenna performance. The behavior below the stable resonance band can be explained by the design of Fig. 2. Below resonance, the armed structure acts like a transmission line where the short-circuited outer band is transformed to an open circuit at certain frequencies.

The results of Fig. 4 are valid for a single set of ε_r and $\tan\delta$. The log-spiral antenna is also simulated with varying ε_r. Due to the use of a DHS, varying a non-zero $\tan\delta$ has no significant effect on the simulation results. Based on Fig. 4, the maximum frequency of this simulation is limited to 20 MHz.

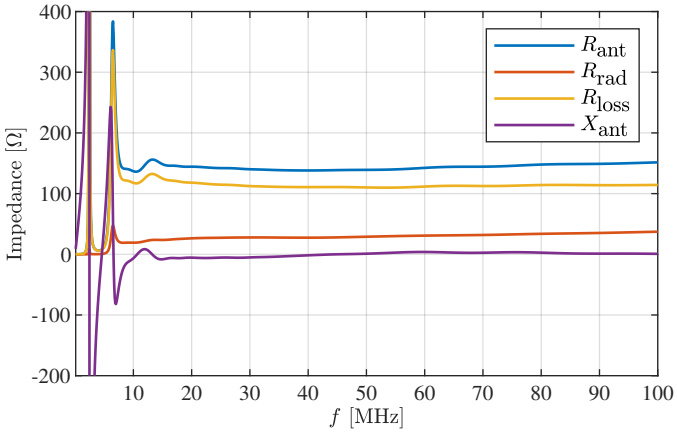

Fig. 4. The complex antenna impedance components of the log-spiral antenna shown in Fig. 2 for 0.1 to 100 MHz.

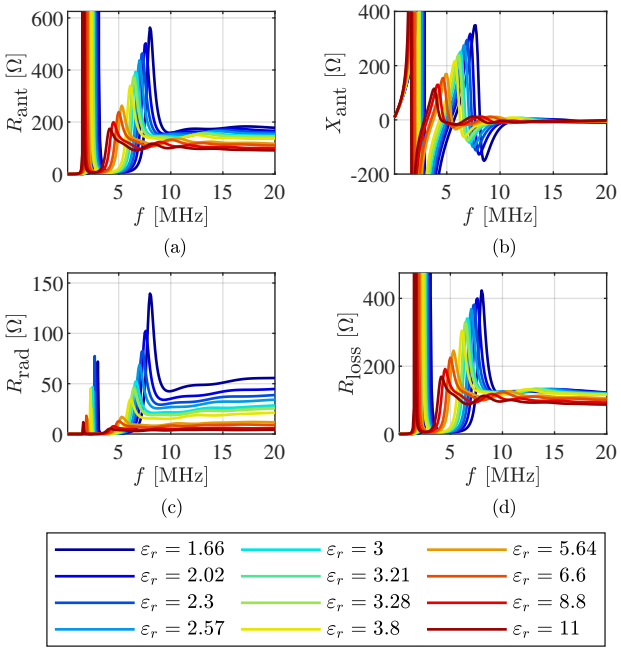

Fig. 5. The complex antenna impedance components (a,b,c,d) of the log-spiral antenna shown in Fig. 2 for various values of ε_r.

Fig. 5 shows the resulting antenna impedance components. The values of ε_r are uniformly selected from an ascending list based on Tab. A9.16 in [11] with the addition of the median $\varepsilon_r = 3.21$. It can be concluded that the flat response is retained for all ε_r but that a high ε_r seriously deteriorates R_{rad}. Next to that, the magnitude as well as the frequency of the open-circuit transformation shifts to lower values for high ε_r.

V. Amplifier Noise Characterization

As discussed in Sec. III-B, lowering the total noise contribution of the receiver is absolutely crucial for the detection of the 21cm-signal. In order to determine the noise voltages required to calculate T_{Rx}, having an accurate noise model of the amplifier when interfaced with the antenna is essential.

In receiver design, the choice is often to use a network representation referred to a common impedance. This allows

to use the overall cascaded Noise Factor (F) or Noise Figure (NF) of the network as an FoM for noise matching. However, a downside of NF is that its value is only valid when the amplifier's input and output are terminated with the reference impedance (i.e. often 50 Ω).

For arbitrary source impedances (e.g. in an active antenna co-design), it is required to know the 4 noise parameters of the amplifier: F_{min}, R_n, $|\Gamma_{opt}|$ and $\angle\Gamma_{opt}$. F_{min} is the minimum F achieved when the input port is matched to optimum source impedance Γ_{opt} and the noise resistance R_n is a measure of how quickly the NF deteriorates when there is a mismatch with respect to $|\Gamma_{opt}|$. With these, it is possible to determine

$$NF = 10\log_{10}\left[F_{min} + \frac{R_n}{G_s}|Y_s - Y_{opt}|^2\right], \quad (5)$$

where G_s is the real part of the source admittance Y_s and Y_{opt} the optimal admittance related to Γ_{opt}.

As accurate amplifier noise models are not available for the frequency range of interest, measurements are required to obtain the noise parameters. Conventional methods require the use of an impedance tuner to sweep the source impedance across the Smith chart. This makes them unsuitable for this work as they become very large and only have a limited operating bandwidth [18]. In [19] the "OSLC method" is introduced which instead uses 3 calibration impedances (i.e. open, short, load) as well as a coaxial cable of length $\frac{\lambda_0}{8}$, where λ_0 is the center wavelength. Replacing the coaxial cable with a capacitor that has the same effect as source impedance, these lumped elements of the "OSLC method" are easier to handle and allow for noise measurements at low frequencies.

A capacitor of 100 pF has been selected to mimic the effect of the coaxial cable. To reduce measurement uncertainty, 5 additional lumped impedances are used: a 330 nH inductor as well as the inductor and capacitor in series with a 27 Ω resistor and in parallel with a 100 Ω resistor. For the measurements, the impedances are placed on a simple printed circuit board.

The selection of amplifiers for the noise measurements is based on Sec. III. In previous designs such as ASTRON's contribution to Netherlands-China Low-Frequency Explorer (NCLE) [20], the electrically small antennas meant that high input impedance amplifiers were favorable to maintain a proper gain [21]. With this legacy, the AD8001a (Analog Devices) and the OPA818 (Texas Instruments) amplifiers were selected. However, the antenna of Sec. IV is not electrically small and thus power match could be possible. Therefore, the PHA-13LN+ (Mini-Circuits) amplifier has been added to the analysis. The main parameters of the amplifier evaluation boards are listed in Tab. II. Note the OPA818 is internally matched to 50 Ω at the input. The AD8001a noise is not included as the custom ASTRON board available for this work does not align with the datasheet.

This setup, combined with [19], allows to determine the noise parameters of an amplifier. All measurements have been repeated 10 times on different days and at different times of day. In order to assess their validity, the obtained noise parameters are used to calculate the standard NF through (5). This value can be compared against the NF of the PHA-13LN+ amplifier mentioned in the datasheet. To enhance the

TABLE II
MAIN AMPLIFIER EVALUATION BOARD PARAMETERS

Parameter	AD8001a	OPA818	PHA-13LN+
Type	Current feedback opamp	Voltage feedback opamp	Regular amplifier
Typ. DC bias	V_S=±5 V	V_S=±5 V	V_S=+3 / +5 V
Typ. gain	23.7 dB	10.9 dB	23.5 / 23.0 dB
Input imp.	∼10 kΩ	∼50 Ω	∼50 Ω
Typ. noise	-	V_n=2.2 nV/$\sqrt{\text{Hz}}$	NF=0.9 dB
OIP3	+33 dBm	+44 dBm	+39 dBm

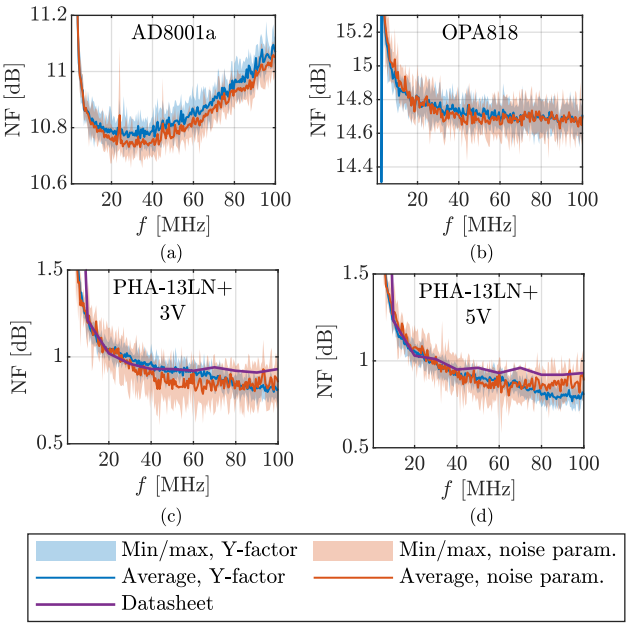

Fig. 6. The noise figure (NF) of the amplifiers in Tab. II (a,b,c,d) calculated using the approach of [19].

NF comparison, the measurement data also allow to calculate the standard NF using the Y-factor method [22]. Fig. 6 shows the resulting minimum, maximum and average NF values. It can be concluded that the two methods seem to show good agreement. Next to that, the measurements align to the datasheet values of the PHA-13LN+ amplifier, keeping in mind it is a different physical device measured with different equipment under different conditions.

VI. Combined Active Antenna Performance

As discussed in Sec. III-B, the equivalent isotropic noise temperature of an active antenna can be used to assess its performance in an astronomical context. This requires combining the results of Sec. IV and V into a single simulation. Fig. 7 shows the simulation schematic as created in the PathWave Advanced Design System software (ADS) [23]. The value of the input noise voltage V_{in} depends on the step of Fig. 1 and only for step 2 were the noise parameters enabled.

Fig. 8 shows the resulting values for T_{Rx} when taking the antenna of Sec. IV and combining it with one of the amplifiers of Sec. V. From the figure, it can be concluded that the AD8001a amplifier and the PHA-13LN+ amplifier for both its biasing settings satisfy the requirement of (1) for the full design frequency range of 10 to 70 MHz. The lower equivalent

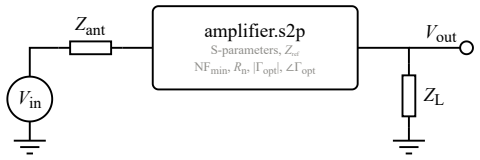

Fig. 7. The simulation schematic corresponding to determining T_{Rx} as outlined in Sec. III-B. The noise parameters are only enabled for step 2.

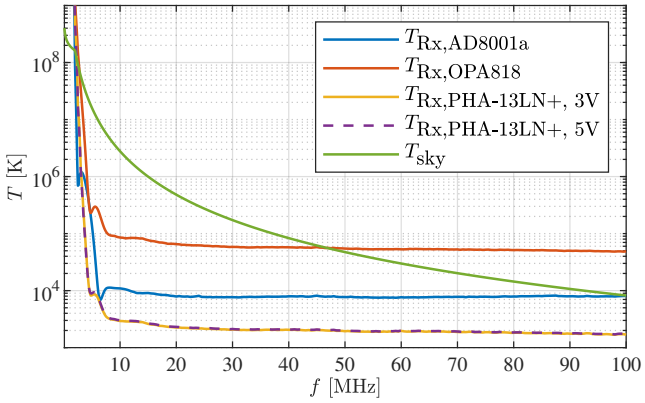

Fig. 8. The equivalent isotropic sky noise temperature and the calculated equivalent isotropic noise temperature of the active antenna combining the log-spiral antenna and an amplifier of Tab. II from 0.1 to 100 MHz.

temperature of the PHA-13LN+ amplifier even means that it stays below 10% of T_{sky} for the full design frequency range.

Next to that, the results of Fig. 8 show that the frequency-independent characteristics of the antenna and amplifier propagate into the calculated T_{Rx}. Again, this shows that the active antenna system satisfies the requirements of Sec. III. The increase in T_{Rx} below approximately 10 MHz can be explained by looking at the antenna radiation impedance shown in Fig. 4. Following (4), R_{rad} converging to 0 Ω has the direct effect that T_{Rx} approaches infinity, irrespective of the value of $V_{\mathrm{out},2}$ and hence irrespective of the amplifier noise characteristics.

VII. Conclusion

In this paper, an active antenna suited to detect the global Dark Ages signal from the far side of the Moon is designed. The strict requirements on frequency-invariant behavior and noise performance resulted in the choice of an equiangular spiral plate antenna connected to the PHA-13LN+ amplifier evaluation board. The simulated equivalent isotropic noise temperature of the active antenna remains below the sky noise from 2.5 MHz up to at least 100 MHz which contains the full design frequency range (10-70 MHz). This shows the system's capability to detect the faint 21cm-line from the Dark Ages or perform other science in this frequency range.

References

[1] A. Loeb, *How Did the First Stars and Galaxies Form?* Princeton University Press, 12 2010.

[2] G. B. Field, "Excitation of the Hydrogen 21-CM Line," *Proceedings of the IRE*, vol. 46, no. 1, pp. 240–250, 1958.

[3] J. O. Burns *et al.*, "A Space-based Observational Strategy for Characterizing the First Stars and Galaxies Using the Redshifted 21 cm Global Spectrum," *The Astrophysical Journal*, vol. 844, no. 1, p. 33, 7 2017.

[4] J. D. Bowman, A. E. Rogers, R. A. Monsalve, T. J. Mozdzen, and N. Mahesh, "An absorption profile centred at 78 megahertz in the sky-averaged spectrum," *Nature*, vol. 555, no. 7694, pp. 67–70, 2 2018.

[5] A. E. Rogers and J. D. Bowman, "Absolute calibration of a wideband antenna and spectrometer for accurate sky noise temperature measurements," *Radio Science*, vol. 47, no. 4, 2012.

[6] S. Singh *et al.*, "On the detection of a cosmic dawn signal in the radio background," *Nature Astronomy*, vol. 6, no. 5, pp. 607–617, 2 2022.

[7] J. Burns *et al.*, "Global 21-cm Cosmology from the Farside of the Moon," *arXiv e-prints*, 3 2021.

[8] M. Klein Wolt *et al.*, "The Astronomical Lunar Observatory (ALO) - Probing the cosmological Dark Ages and Cosmic Dawn with a distributed low-frequency radio array on the Lunar Far Side," Paris, 9 2022.

[9] N. Bassett, D. Rapetti, J. O. Burns, K. Tauscher, and R. MacDowall, "Characterizing the radio quiet region behind the lunar farside for low radio frequency experiments," *Advances in Space Research*, vol. 66, no. 6, pp. 1265–1275, 9 2020.

[10] M. Robinson, "Farside! And all the way around," 3 2011. [Online]. Available: http://lroc.sese.asu.edu/posts/298

[11] G. H. Heiken, D. T. Vaniman, and B. M. French, *Lunar Sourcebook*. Cambridge University Press, 1991.

[12] S. Jester and H. Falcke, "Science with a lunar low-frequency array: From the dark ages of the Universe to nearby exoplanets," *New Astronomy Reviews*, vol. 53, no. 1-2, pp. 1–26, 5 2009.

[13] J. O. Burns *et al.*, "Probing the first stars and black holes in the early Universe with the Dark Ages Radio Explorer (DARE)," *Advances in Space Research*, vol. 49, no. 3, pp. 433–450, 2 2012.

[14] Altair, "Altair Feko," 2020. [Online]. Available: https://altair.com/feko-applications/

[15] J. D. Dyson, "The Equiangular Spiral Antenna," *IRE Transactions on Antennas and Propagation*, vol. 7, no. 2, pp. 181–187, 1959.

[16] R. Bawer and J. Wolfe, "The spiral antenna," *IRE International Convention Record*, pp. 84–95, 3 1960.

[17] Dassault Systèmes, "Antenna Magus," 2023. [Online]. Available: https://www.3ds.com/products-services/simulia/products/antenna-magus/

[18] M. Himmelfarb and L. Belostotski, "On impedance-pattern selection for noise parameter measurement," *IEEE Transactions on Microwave Theory and Techniques*, vol. 64, no. 1, pp. 258–270, 1 2016.

[19] D. C. Price, C.-Y. E. Tong, A. T. Sutinjo, L. J. Greenhill, and N. Patra, "Measuring Noise Parameters Using an Open, Short, Load, and 1/8-wavelength Cable as Source Impedances," *IEEE Transactions on Microwave Theory and Techniques*, 10 2022.

[20] M. J. Arts, D. S. Prinsloo, M. Ruiter, and A. J. Boonstra, "Design of a reconfigurable array of monopoles for the Netherlands China Low-frequency Explorer," *European Conference on Antennas and Propagation*, 2019.

[21] K. F. Warnick and M. A. Jensen, "Signal and noise analysis of small antennas terminated with high-impedance amplifiers," *IET Seminar Digest*, vol. 2007, no. 11961, 2007.

[22] Keysight Technologies, "Noise Figure Measurement Accuracy: The Y-Factor Method," Keysight Technologies, Santa Rosa, CA, USA, Tech. Rep., 1 2021.

[23] ——, "PathWave Advanced Design System (ADS)," 2023. [Online]. Available: https://www.keysight.com/us/en/products/software/pathwave-design-software/pathwave-advanced-design-system.html